

INVESTIGATION OF THE ROLE OF DUCTILITY IN THE ASSESSMENT OF STRUCTURES UNDER TSUNAMI LOADING

Joshua MACABUAG¹, Crescenzo PETRONE², Tiziana ROSSETTO³

ABSTRACT

This paper investigates the fundamental principle of whether ductility and dynamic effects are significant in determining structural performance under tsunami loading. It is first shown analytically that an Elastic-Perfectly-Plastic (EPP) Single Degree of Freedom (SDoF) can maintain a load (F) greater than its yield load (F_y) for a duration of time. For an idealised triangular load, the overstrength factor (F/F_y) scales with the displacement ductility demand according to dimensionless parameters of (a) ratio of F_y to the peak applied load, and (b) the ratio of natural period to the duration for which the load exceeds yield. Finally, it is shown that for realistic tsunami load time-histories that the structure will collapse if the applied loads exceed F_y for any significant time. The implications for tsunami-resistant design are that structures must be designed to withstand the full tsunami load elastically and therefore that static procedures could be sufficient for their assessment. The implication for catastrophe modelling is that analytical fragility and vulnerability functions may also be derived using static procedures.

Keywords: Tsunami; Ductility; Structural Dynamics

1 INTRODUCTION

Tsunami have the potential to cause enormous life and financial losses, as demonstrated by the 2011 Great East Japan Earthquake and Tsunami and the 2004 Indian Ocean Tsunami (Guha-Sapir et al. 2015). Central to tsunami risk mitigation is the protection of critical infrastructure and evacuation buildings, which are all necessarily within tsunami inundation zones and must be designed to withstand tsunami loading. Current tsunami design guidance (e.g. Japanese guidance MLIT 2570 and US ASCE 7-16) requires these critical structures to be designed to resist elastically one or more tsunami loading combinations that are assumed to occur at specific points along a tsunami inundation time-history (e.g. at point of maximum momentum flux and other points). This elastic design criterion reflects the importance of these critical structures, which must remain functional after a tsunami, but also the fact that the study of tsunami forces and impacts on structures is a relatively new field, and that significant uncertainties still exist.

Whilst it is acceptable for design standards to be inherently conservative for critical infrastructure, in the context of very rare but very significant hazards, like tsunami and earthquakes, the extension of this conservatism to the design of normal residential or industrial buildings can potentially result in very expensive designs. In the case of seismic building codes this is addressed by introducing the concept of capacity design, which allows the structure to resist some of the earthquake loads through plastic deformation. The maximum amount of plastic deformation that the structure can sustain whilst still maintaining its vertical load carrying capacity is represented by its structural ductility supply (μ = ratio of ultimate deformation to yield deformation). The word ‘supply’ is used here to distinguish the capacity of the structure from the ‘demand’ placed on it by the earthquake. In the codes, the structural ductility supply is related to an over-strength factor (i.e. the ratio of applied load to the structural yield

¹NatCat R&D Analyst, SCOR, London, UK, macabuag@gmail.com

²Earthquake Research Analyst, Willis Towers Watson, UK

³Professor and Director of the Earthquake and People Interaction Centre (EPICentre), University College London, UK

strength, $\Omega = F(t)/F_y$), which is utilized to reduce the seismic design loads. This results in a more

economic upfront design cost, and life-safety in cases where an earthquake occurs that deforms the building to within its ductility supply limit. In the latter case, the cost of repair or rebuilding of the structure is assumed acceptable given the low frequency of such earthquake events.

The basis of these assumptions in seismic design derives from fundamental structural dynamics. As a structure deforms under a time-dependent load, it develops inertia forces, damping forces and internal (spring) forces (Figure 2). However, in contrast to the earthquake engineering literature, to date very limited attention has been given to the areas of structural damping, ductility, overstrength and other time-dependent effects by the tsunami research community. This paper therefore looks to investigate whether it is possible to utilize a structure's damping and ductility supply for the development of a significant overstrength that can be exploited in the tsunami design of buildings.

Like earthquakes, tsunami inundation flows impose a time-varying load on structures, with a strong horizontal force component. However, the load time-history areas over which the load is applied and the duration of this horizontal loading are very different. The leading edge of a tsunami wave inundates the land generally in the form of a surge, or under certain conditions, as a hydraulic bore. In the context of tsunami inundation, a surge describes the motion of unbroken wave runup over a dry bed, or the swelling or rising of water level over standing water. A bore does not always form, but when it does it is a broken wave with a steep, turbulent wave front, which propagates over quiescent water of a finite depth (Robertson and Riggs, 2011). As tsunami waves tend to break offshore or near-shore, loads imposed by bores are generally not applicable to onshore buildings away from the surf zone (Yeh et al. 2014). Due to the very long wave period of tsunamis, after impingement of the initial surge or bore, tsunami runup becomes quasi-steady (i.e. changes in flow parameters are slow, such that force components due to accelerations of the flow are negligible). Tsunami inundation flows are therefore thought to result in the general pressure time-history shown in Figure 1, where the impulsive bore impact pressure may or may not be greater than the sustained (quasi-steady) pressure (Arikawa et al. 2012; Nistor et al. 2010; Nouri, 2008; Nouri et al. 2010). This initial impulsive pressure, whilst commonly observed for waves impinging on walls and for short to long waves impacting buildings, is not seen in recent physical experiments of very long, tsunami-like waves impinging on structures (Foster et al. 2017). Hence several recent studies have tended to ignore the initial impulse (Petrone et al. 2017; Qi et al. 2014). Despite these observations, it is not yet clear as to whether the problem of structural analysis under tsunami loading should be treated as a dynamic problem or not.

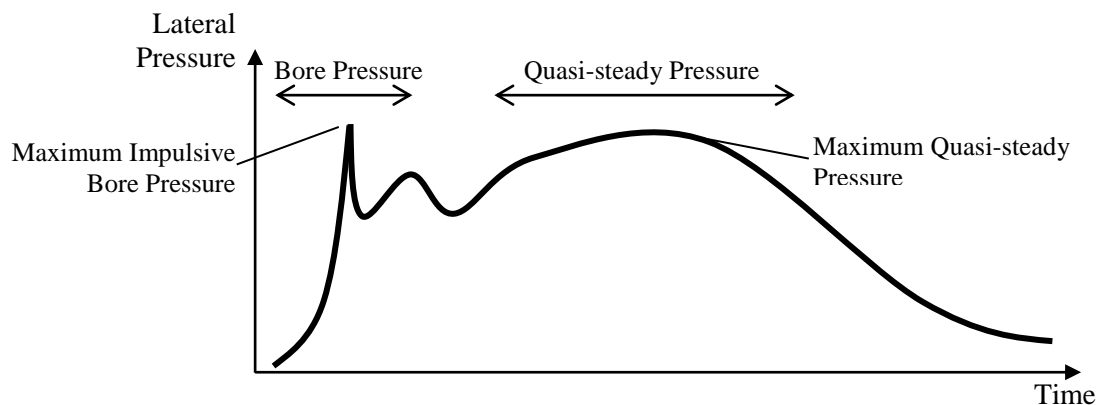


Figure 1. Typical load time-series for single bore impingement on an onshore structure, showing initial impulsive bore impact pressure followed by a sustained (quasi-steady) pressure (after Arikawa et al. 2012)

Published studies adopt a number of techniques for structural analysis under tsunami loading that vary in complexity from time-history analysis of a 3D structural model (Chock et al. 2013), to simple mechanics-based models that consider particular failure mechanisms (Dias et al. 2009). Different assumptions are also made on how the pressure/forces imparted by the tsunami flow should be applied to the structure analysed. Macabuag and Rossetto (2014) and Petrone et al. (2017) show that the structural

response to tsunami loading is very sensitive to the distribution in elevation of the applied tsunami pressure. Although ASCE 7-16 (2017) and FEMA 646 (2012) recommend uniform distribution of pressure in elevation, recent studies show that a linear (triangular) vertical distribution for drag-induced pressures might be more appropriate (Petrone et al. 2017). Furthermore, Petrone et al (2017) compares the results of time-history analyses and non-linear static analyses of a 2D structural model and demonstrates that a novel varying height pushover approach provides an appropriate simplified analysis technique for the determination of structural response of engineered buildings under tsunami loading. The fact that a pushover type analysis can represent the structural response of a building under a tsunami time history implies the structure has a predominant response that can be represented by a single-degree of freedom system. Such an assumption is made by Park et al. (2012) in their structural idealization for the study of sequential earthquake and tsunami load effects on buildings.

This paper presents the results of a study that aims to quantify the duration over which a structure can sustain a load greater than its yield load (F_y) for tsunami type load histories. This is first investigated analytically for an undamped, Elastic-Perfectly-Plastic (EPP) Single Degree of Freedom (SDoF) system (Figure 2 with $c=0$, $b=0$) subjected to a number of idealized tsunami load histories. The analytical results are then verified numerically, before extending the analysis to consider structural damping and strain-hardening. Next, the SDoF behaviour is investigated under realistic tsunami load time-histories obtained from numerical inundation modelling. The implications of the results for the assessment and design of buildings subjected to tsunami is discussed, and wider questions are raised on the treatment of structures subjected to sequential earthquake and tsunami loads.

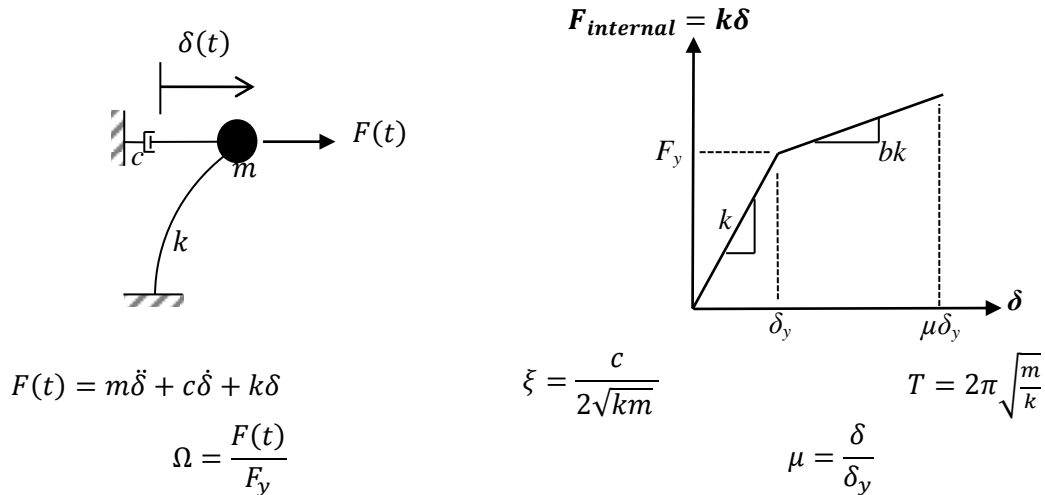


Figure 2. Equation of motion, performance curve, and terminology for a SDoF structure used throughout this study. m = structural mass. c = damping. c_c = critical damping. k = stiffness. ξ = damping ratio. b = strain-hardening ratio. T = natural period of vibration.

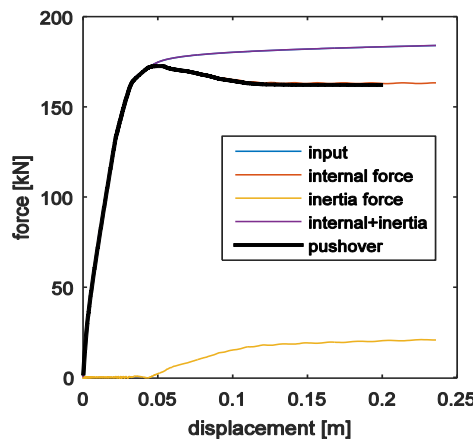


Figure 3. General performance curve of a structure loaded beyond yield.

2 OVERSTRENGTH VS DUCTILITY RELATIONSHIP FOR AN ELASTIC PERFECTLY-PLASTIC STRUCTURE

2.1 Analytical Derivation

This section investigates whether structural overstrength (Ω) and displacement ductility demand (μ) under time-varying load ($F(t)$) can be determined analytically, so that the peak displacement ductility demand (μ_{peak}) for a structure under a given load time-history can be predicted.

Initially, an undamped, elastic-perfectly-plastic (EPP), single degree-of-freedom (SDoF) structure of mass, m , is considered, as shown in Figure 2. Once the applied force exceeds the yield force of the structure, F_y , then the structure will behave plastically, and so a subscript p shall be used to denote variables measured from the yield-point onwards (e.g. $F_p = F - F_y$, $t_p = t - t_y$, etc). The dynamic behaviour is governed by the standard equation of motion with damping and stiffness coefficients both zero (Figure 2, $c=0$, $k=0$). In the post-yield (plastic) region for the EPP structure the internal force remains at F_y , and so the acceleration of the structure is determined by the net force ($F - F_y = F_p$) as shown in (1). The plastic velocity and plastic deflection ($\delta_p(t) = \delta(t) - \delta_y$) are then found by integration (2).

$$\ddot{\delta}_p(t_p) = \frac{F_p(t_p)}{m} \quad (1)$$

$$\delta_p(t_p) = \frac{1}{m} \iint F_p(t_p) dt_p^2 \quad (2)$$

Equations for overstrength and ductility, with respect to time, both follow from the definitions of these parameters (3) (4). It is highlighted that the plastic displacement ductility demand, μ_p , is a function of the applied load, the yield force, and the natural period of the structure, T (defined by: $= 2\pi \sqrt{\frac{m}{k}}$). It

is observed from equation (4) that the natural period of the structure influences the ductility demand as it contains information about both the structural mass (which governs acceleration) and structural stiffness (which governs the deflection at yield).

$$\Omega_p(t_p) = \frac{F_p(t_p)}{F_y} \quad (3)$$

$$\mu_p(t_p) = \frac{\delta_p(t_p)}{\delta_y} = \frac{\frac{1}{m} \iint F_p(t_p) dt_p^2}{F_y/k} = \left(\frac{2\pi}{T}\right)^2 \frac{1}{F_y} \iint F_p(t_p) dt_p^2 \quad (4)$$

The overstrength-ductility relationship is evaluated for three load time-histories: a linearly increasing load (Figure 4a); a triangular forcing function where the gradients of the upward and downward ramps are equal (Figure 4b); and a parabolic forcing function (Figure 4c).

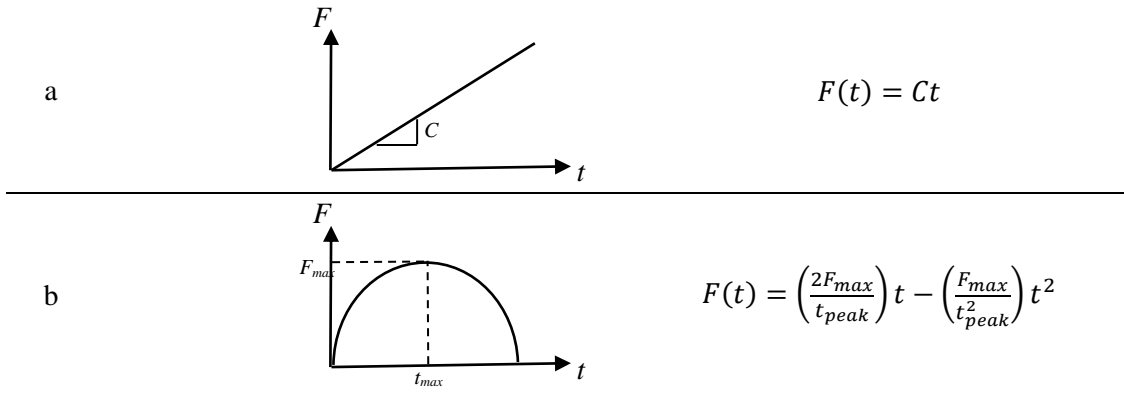


Figure 4: General definitions of the three load-cases applied: (a) a linearly increasing load, (b) a triangular forcing function, and (c) a parabolic forcing function.

For an EPP structure under a linearly increasing forcing function (Figure 4a), the overstrength and ductility with respect to time can be calculated from (3) and (4), to give the relationships shown in (5) and (6). A direct relationship between overstrength and ductility ($\Omega_p(\mu_p)$) can then be found as shown in (7). This equation shows that structures with the same ratio of T/F_y should have identical Ω_p - μ_p curves when subjected to the same linearly increasing load.

$$\Omega_p(t_p) = \frac{C t_p}{F_y} \quad (5)$$

$$\mu_p(t_p) = \left(\frac{2\pi}{T}\right)^2 \frac{C}{6F_y} t_p^3 \quad (6)$$

$$\Omega_p = A \mu_p^{1/3} \quad ; \quad A = \left(\frac{C\sqrt{3}}{\pi\sqrt{2}}\right)^{2/3} \cdot \left(\frac{T}{F_y}\right)^{2/3} \quad (7)$$

For an EPP structure under a parabolic forcing function (Figure 4b) which exceeds the yield force for a duration of time ($t_{dur} = 2t_{p_{peak}}$), plastic overstrength follows directly from the definition of the forcing function (8). Using the same method as for linear ramps above, plastic ductility demand is expressed as in (9). It is highlighted here that the structural deflection will continue to increase even after the applied force has reduced back to values below the yield force, due to the developed inertia. The peak deflection is therefore defined when $\dot{\delta}_p = 0$, giving rise to the analytical definition of peak deflection ductility demand shown in (10).

$$\Omega_p(t_p) = 4 \frac{\Delta F_{max}}{F_y} \left[\left(\frac{1}{t_{dur}}\right) t_p - \left(\frac{1}{t_{dur}^2}\right) t_p^2 \right] \quad (8)$$

$$\mu_p(t_p) = \frac{1}{3} \left(\frac{2\pi}{T}\right)^2 \frac{\Delta F_{max}}{F_y} \left[\left(\frac{2}{t_{dur}}\right) t_p^3 - \left(\frac{1}{t_{dur}^2}\right) t_p^4 \right] \quad (9)$$

$$\mu_{p \max} = \mu_p(t_{p_{\dot{\delta}=0}}) = \frac{9}{4} \pi^2 \Omega_{p_{peak}} \left(\frac{t_{dur}}{T}\right)^2 \quad (10)$$

Equation (10) shows that under parabolic loading, the maximum ductility demand (μ_{max}) is determined by only two dimensionless parameters:

$$\left(\frac{t_{dur}}{T}\right), \left(\frac{\Delta F_{max}}{F_y}\right)$$

where $\Delta F_{max} = F_{max} - F_y$.

2.2 Numerical Verification of Analytical Formulae

This section compares the analytically derived overstrength and ductility relationships with numerical results. Structural analyses are carried out in OpenSees (McKenna et al. 2010) on 7 SDoF structures with different properties, but all with bilinear response curves (Table 1). All subsequent analyses of OpenSees results are conducted in the statistical programming language R (R Development Core Team, 2008). The analytical equations of the previous section are tested against numerical simulations for the SDoF's of Table 1. However, only the results for structure S3 ($F_y=10\text{kN}$, $T=1\text{s}$) are shown for brevity, except where noted.

Equation (7) suggests that EPP structures with the same ratio (T/F_y) should have identical Ω - μ curves when subjected to the same linear ramp forcing function. To test this, the SDoFs in Table 1 are defined such that they can be grouped into three different (F_y/T) ratios, and are subjected to a linear ramp forcing function (Figure 4a, with $C=1\text{kN/s}$). Also, as (4) suggests that the natural period, T , is sufficient for capturing information about the structural mass and stiffness, structures S3 and S4 are defined to have identical periods, but with different mass and stiffness values.

Table 1. Structures to be considered in this study. Structure S3 is highlighted as it will be the base-case structure used throughout this paper. All structures are initially considered with no damping.

Structure Number	F_y (kN)	T (s)	Mass (tons)	k (kN/m)	F_y/T
S1	5	1	14	553.6	5
S2	7.5	1.5	31.6	553.6	5
S3	10	1	14	553.6	10
S4	10	1	8.2	325.2	10
S5	5	0.5	3.5	553.6	10
S6	10	0.5	3.5	553.6	20
S7	20	1	14	553.6	20

Figure 5 shows the response of structure S3 subjected to the linear ramp forcing function. Figure 5a shows that post-yield the applied force is resisted by the internal (i.e. spring) force of the structure (which remains at F_y for an EPP structure) plus the inertia force of the yielded structure, as hypothesised in Figure 2. This results in the structural displacement and acceleration illustrated in Figure 5b, where the analytical and numerical results are shown to be in good agreement. Figure 5c also shows good agreement between the numerical and analytically derived overstrength vs ductility relationships. Minor discrepancies are observed because the assumptions of zero velocity and acceleration at the yield point are not true, particularly in the case of no damping. Furthermore, it is not always true that $\Omega=1$ when $\mu=1$ (due to the dynamic oscillations of the structure in the elastic region), which again produces discrepancies between the analytical predictions and numerical results.

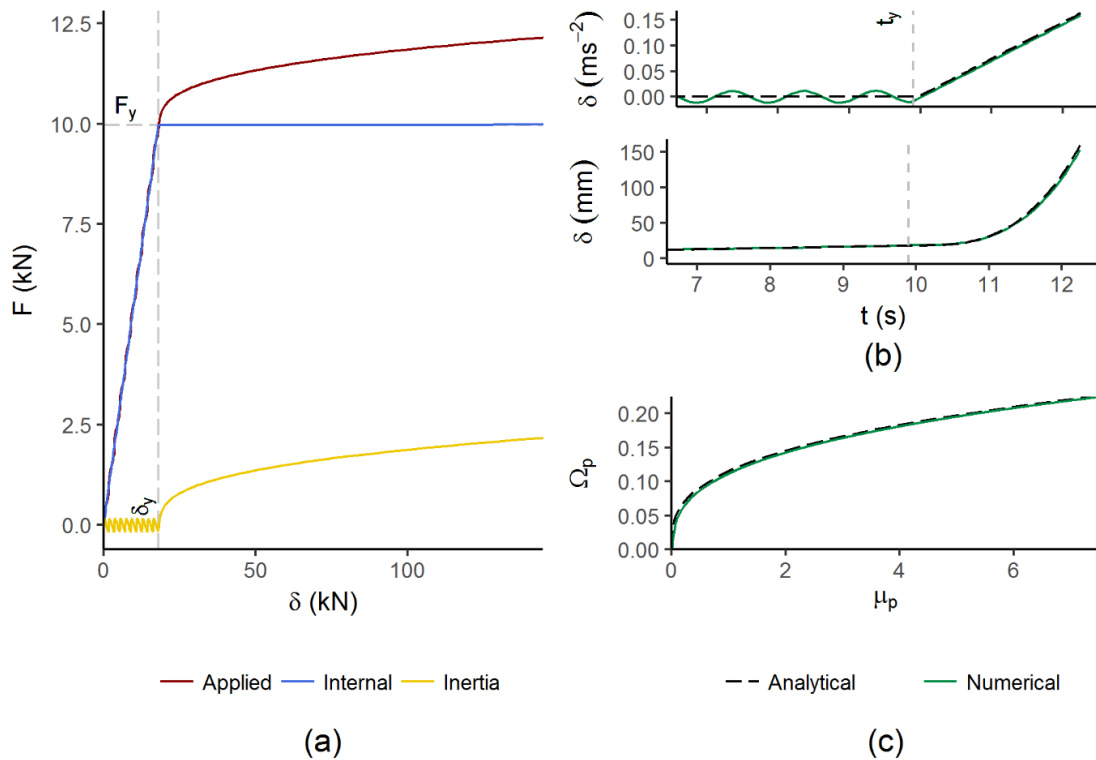


Figure 5. Responses of structure S3 (Table 1) subjected to a linear ramp forcing function (Figure 4a) with $C=1\text{kN/s}$. (a) performance curve (dashed vertical lines indicate $\mu=1:8$). (b) analytical and numerical comparison of structural motion vs time. (c) analytical and numerical comparison of overstrength vs ductility relationship.

Figure 6 shows the overstrength vs ductility relationships for all seven structures of Table 1. As expected, structural responses collapse onto three curves defined by the three F_y/T ratios. In addition, the response curves for structures S3 and S4 are identical despite having different masses and stiffness,

demonstrating the general conclusion that structural period, T , is indeed sufficient for capturing the structural behavior, as predicted by (7).

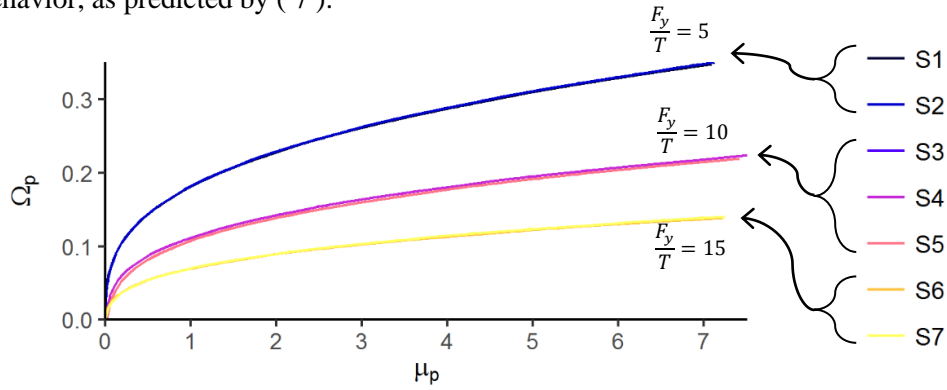


Figure 6. Seven test structures subjected to a linear ramp forcing function (Figure 4a, with $C=1\text{kN/s}$). The $\Omega_{plastic}$ vs $\mu_{plastic}$ responses collapse onto 3 curves, defined by F_y/T ratio.

Figure 7 compares the analytically and numerically derived response of S3 subjected to a parabolic time-history defined by Figure 4b, with $C=1\text{kN/s}$ and $F_{max}=11\text{kN}$. Figure 7b shows a good match between the analytical and numerically derived the overstrength vs ductility relationship. The analytical results slightly underestimate peak ductility demand. This is due to a number of reasons. The analytical model assumes negligible acceleration and velocity prior to yield ($\delta_p(t) = \dot{\delta}(t) = 0, t < t_y$), though the numerical model may have non-zero acceleration and velocity at the yield point, giving rise to the slight discrepancy between deflections shown. In addition, the point of yield (t_y) is not coincident for the numerical and analytical models. For the numerical model yield occurs where the structure's internal (spring) force exceeds F_y , where the internal force differs from the applied force due to inertial and damping loads (though $\zeta=0$ in this case). However, the analytical model assumes no inertia or damping forces (as $\delta_p(t) = \dot{\delta}(t) = 0, t < t_y$), and so implicitly assumes yield at the point where the applied load exceeds F_y .

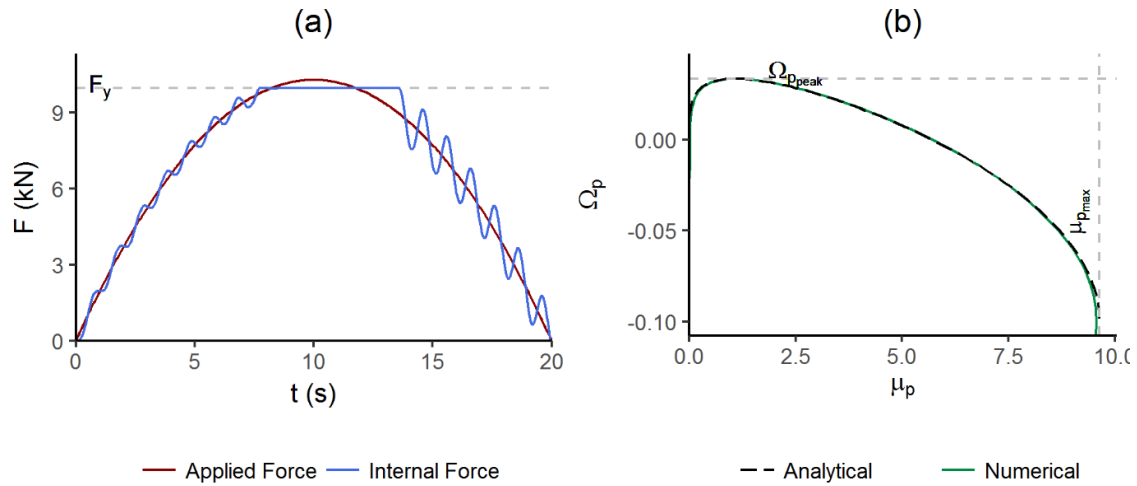


Figure 7. Responses of structure S3 (Table 1) subjected to a parabolic forcing function (Figure 4c) with $F_{max}=10.3\text{kN}$. (a) applied and internal force w.r.t. time. (b) analytical and numerical comparison of overstrength vs ductility relationship.

2.3 Overstrength Envelope

The previous section has shown the analytical estimations of structural performance to be in agreement with numerical results. Therefore, if parabolic load time-histories can be considered representative of tsunami loading then for a given undamped EPP structure (defined by F_y, T) under a

given tsunami loading (defined by ΔF_{max} , t_{dur}) the peak ductility demand can be calculated from (10), and the structure is deemed to have failed if $\mu_{demand} > \mu_{supply}$. Therefore, (10) can also be used to define the relationship between peak plastic overstrength demand ($\Omega_{p_{peak}}$) and the duration for which the applied load exceeds the yield load non-dimensionalised by the structural period ($\frac{t_{dur}}{T}$), for a series of target peak plastic ductility demands ($\mu_{p_{max}}$). These analytical relationships for $\mu_{p_{max}} = 1:8$ are shown in Figure 8.

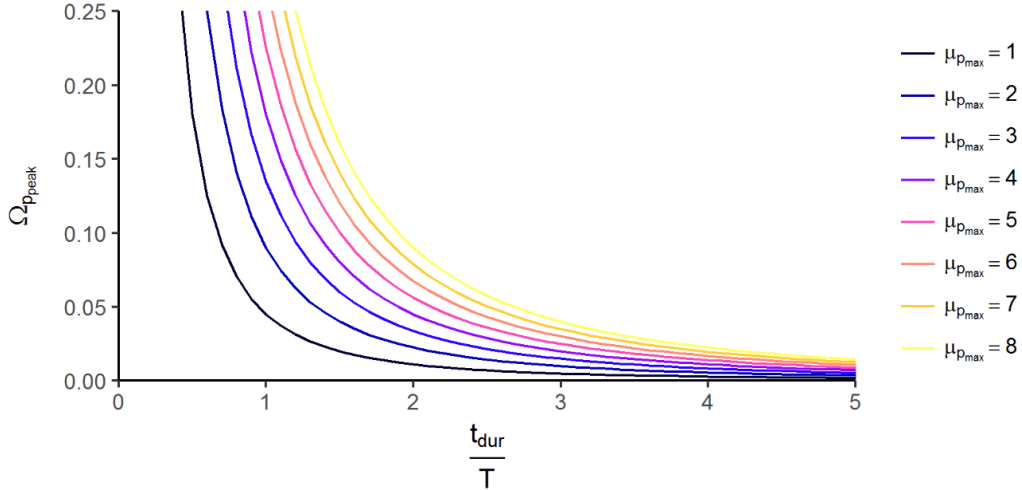


Figure 8. $\Omega_{p_{peak}}$ vs (t_{dur}/T) curves for $\mu_{p_{peak}} = [1:8]$ (defined by Error! Reference source not found.) for an undamped EPP structure.

Figure 8 shows that structures can only achieve an overstrength greater than 5% when subjected to loads which exceed the structural yield load for a duration of between 1 to 3 times its natural period. If typical natural periods are in the range 0.1s-1s then this allows for yield exceedance for between 0.1s and 3s. This overstrength cannot therefore be utilised by structures during the quasi-steady period of the tsunami load time-history (Figure 1), as the duration of this loading phase will exceed the allowable durations defined in Figure 8 for the overwhelming majority of cases. However, the relationships identified here may be of design significance for structures experiencing bore impact (Figure 1), which may well be within the allowable durations defined in Figure 8. For these rapidly applied load-cases, however, it will be necessary to make some compensation for the structural oscillations experienced in the elastic pre-yield period.

3 SENSITIVITY ANALYSIS

The previous section showed that undamped EPP structures are only able to utilise ductility and overstrength to resist highly transient loads. In order to investigate whether the demonstrated overstrength relationship is significant for structures subjected to realistic tsunami time-histories, numerically-derived load time-histories are applied to the SDoF structure S3 (Table 1) with varying levels of strain-hardening and damping (Table 2). For brevity only the results of structure S3 are presented below, though the results have been shown to be valid for all of the SDoFs of Table 1.

For a damped structure, after yield has occurred, the difference between the applied force and the structure's internal (spring) force is resisted by both structural inertia and damping. Damped structures accelerate more slowly than undamped structures, and so increased damping corresponds to an increased overstrength achieved for a given ductility demand. When these same structures are subjected to a load which exceeds yield for a finite amount of time structural damping slows the structure movement reducing the peak displacement and so peak ductility demand. When strain-hardening is introduced, after yield the structure oscillates about the plastic hardening line of its performance curve. It is expected that damping and strain-hardening both reduce the peak ductility

demand imposed on a structure by a time-varying load.

The assumed parameters in this calculation are given in Table 2. It is noted that mechanisms of damping differ under seismic and tsunami loading. A structure undergoing cyclic seismic loading will experience hysteretic damping, where energy is dissipated plastically as the structure cycles through hysteresis loops. As tsunami loading results in far fewer load reversals, there is minimal hysteresis, and so damping is predominantly viscous (e.g. friction in connections and cladding, bond-slip and cracking in RC structures, and damping associated with soil and foundations). Whereas seismic design and analysis tends to assume a damping ratio of approximately 5% for reinforced concrete structures and 2% for steel structures, there are no studies which investigate the sensitivity of tsunami structural response to the presence of damping, and what suitable values might be. Here values of 0 and 5% damping are assumed as plausible limits to expected damping values.

Table 2. The structural parameters for equivalent nodal load calculation and numerical analysis illustrated in this section, Figure 14 and 15. For this example, a flow blocking ratio of 0.6, a loading width of 2m and uniform lateral pressure distribution are assumed.

Structure (Table 1)	μ_{max}	l	b	ζ
S3.1	8	4m	0	0%
S3.2			0	5%
S3.3			0.05	0%
S3.4			0.05	5%

Inundation depth and velocity time-histories are obtained from the numerical inundation simulations of Petrone et al. (2017), which are converted into force time-histories using the equations for force in Qi et al. (2014) assuming a blockage ratio of 0.6. Figure 9 shows a representative tsunami time-history and the corresponding responses of the structures in Table 2. For the structure without strain hardening (S3.1, S3.2 in Table 2), the structure fails shortly after the yield load is exceeded, and long before the applied load can drop back below yield. The presence of ductility in the structure is insufficient for preventing or significantly slowing structural failure. However, structures with strain-hardening (S3.3, S3.4 in Table 2) continue to maintain the increasing load beyond yield, over the duration for which it is applied. For the structures which strain-harden, velocities and accelerations (and so damping and inertia forces) remain close to zero.

The record shown in Figure 9 demonstrates the general result, that realistic tsunami time-histories are very unlikely to exceed the yield force of an EPP structure, or ultimate load capacity of a strain-hardening structure, for a short enough duration for ductility to prevent collapse. The presence of damping does not significantly change this result for realistic tsunami time-histories. This agrees with the very short allowable durations indicated by Figure 8.

If dynamic effects can be ignored then from the definitions of plastic overstrength, plastic ductility and the strain-hardening ratio (Figure 2) it is trivial to show that the static overstrength-ductility relationship is given by (11). Figure 10 shows a comparison between the peak ductility demand predicted from this static relationship and that obtained from numerical analysis for structures with a range of strain-hardening ratios. Generally, (11) is shown to predict the peak ductility demand well, with the greatest accuracy obtained for structures with higher strain-hardening ratios.

$$\Omega_p = b\mu_p \quad (11)$$

This appears to confirm that dynamic affects do not greatly influence the post-yield behavior for strain-hardening structures. Additionally, as the ductility demands shown in Figure 10 are unrealistically high for most structures considering realistic strain hardening ratios, the conclusion made previously that the overstrength and ductility of a structure cannot be relied upon for tsunami-resistant design of structures is confirmed.

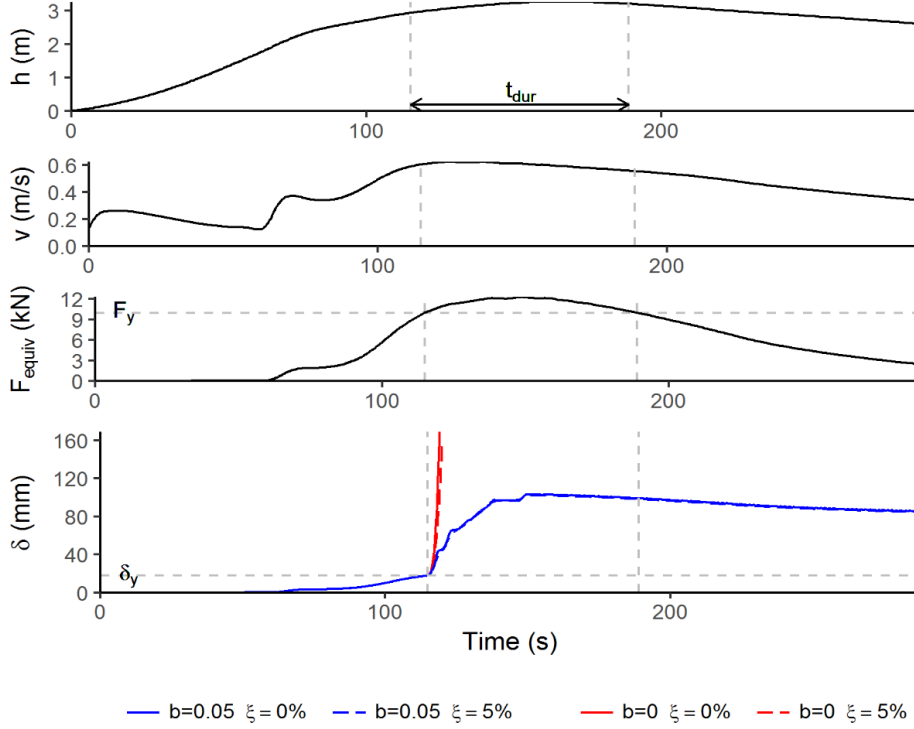


Figure 9. Structural response under a numerically-derived inundation time-history. (a) Inundation depth (h), velocity (v), equivalent nodal force (F_{equiv} , calculated as per Error! Reference source not found.), and structural displacement (δ). (b) Force vs structural displacement for structure S3.1 (top) and S3.2 (bottom) (as per Table 2)

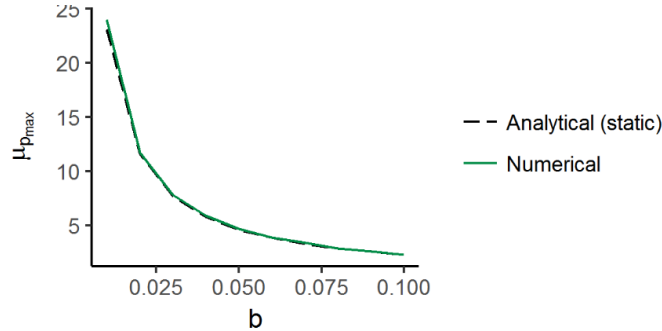


Figure 10. Comparison of static analytical prediction of peak plastic ductility demand ($\mu_{p,max}$) with dynamic numerical results. The analysed structures are based on S3 (Table 1) with a range of strain-hardening ratios (b), subjected to the tsunami time-history shown in Figure 9.

4 CONCLUSIONS AND IMPLICATIONS OF RESULTS FOR THE DESIGN AND ASSESSMENT OF STRUCTURES UNDER TSUNAMI LOADING

It has been shown analytically that an EPP SDoF structure can maintain a load greater than its yield load (F_y) for a duration of time, and that peak displacement ductility demand (μ_{peak}) for a SDoF EPP structure is related to two dimensionless parameters, where the relationship $\mu_{peak} \left(\Omega_{p,peak}, \left\{ \frac{t_{dur}}{T} \right\} \right)$ has been defined analytically for tsunami loading idealised as triangular and parabolic time-histories. It has also been shown that for realistic values of t_{dur} and T , the peak overstrength realised is negligibly small, and so dynamic effects may be ignored for the purposes of design and damage assessment of buildings subjected to tsunami inundation. This result is upheld for a SDoF structure with strain-hardening (idealised by a bilinear performance curve). In this case the ultimate ductility demand placed on a bilinear SDoF structure can be defined by the strain hardening ratio (b) and the required overstrength. However, for real structures with limited strain hardening and ductility supply, the amount of overstrength provided is almost negligible.

These results imply that, with the exception of global failure due to bore impact, structures must be designed such that their maximum strength is greater than the load applied by the design tsunami; typically achievable structural ductility limits do not allow for reliance to be made on overstrength. The building maximum lateral strength under tsunami inundation loads can be determined from a variable height pushover analysis as suggested in Petrone et al. (2017), which takes into account the lateral load distribution imposed by a tsunami inundation (albeit with significant assumptions). It is highlighted here that due to differences in the distribution of lateral loads applied by tsunami inundations as compared to earthquakes, the maximum lateral strength under the individual hazards is significantly different, with structures often displaying a higher strength under tsunami loading distributions than under earthquake loading distributions (Macabuag et al., 2014).

As maximum strength is found to govern the tsunami design of buildings, in seismic areas the potential for an earthquake to precede the tsunami should be considered. In the case of structural assessment under earthquake and tsunami, a reduced strength under the tsunami loading should be considered to account for preceding earthquake damage. The determination of this strength requires a deeper investigation, but the concept is shown schematically in Figure 16, where $F_{t\ max}$ indicates the maximum tsunami strength of the building, $F_{t\ max\ |DS=n}$ is the reduced tsunami strength due to a preceding earthquake bringing the structure to damage state n . In Figure 16, earthquake damage is assumed to precede the tsunami inundation and a nominal earthquake damage scale is used where DS0 represents no damage, DS1 slight damage, DS2 light damage (and the threshold of structural yield in an earthquake), DS3 moderate damage, DS4 extensive damage and DS5 collapse. The red thresholds delimit the collapse limit state and the arrows show a progression of damage from the original earthquake damage state to that in the building when the tsunami force exceeds the tsunami resistance capacity of the building. It is highlighted that, as the ductility of the structure is not utilized the structure may not pass through all the traditionally defined earthquake damage states (e.g. extensive damage level) before collapse under tsunami loading. In the case of the design of critical infrastructure, the results of this study imply that no strength degradation due to earthquake damage is allowed and structural ductility demand might be significantly limited for the earthquake load case. In cases where the seismicity at the facility location is dominated by a tsunamigenic earthquake source, this requirement on seismic design may be more severe than implied by current seismic codes. The reason for this is that the latter account for the structural importance by effectively increasing the return period of the earthquake for which they are designed, but still allow for earthquake load reduction under this event through ductility consideration. Here, reliance on ductility might not be allowed and for the critical facility to be functional after the tsunami, the structure should be designed to resist the expected earthquake loading elastically as well as resisting the full tsunami force. This is likely to result in very expensive designs but the expense may be justified by the essential nature of the critical infrastructure.

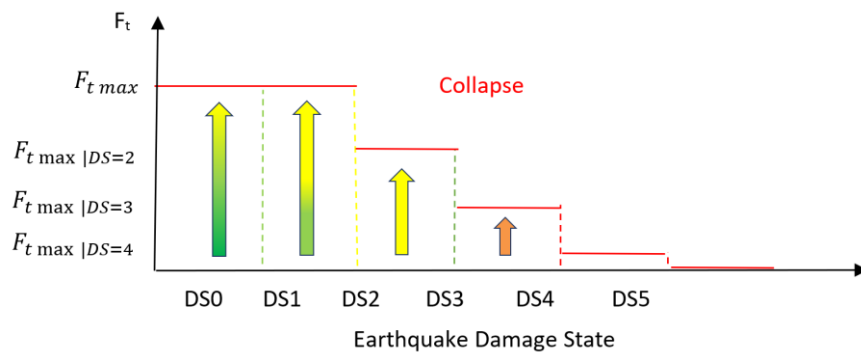


Figure 16. Schematic showing the reduced tsunami collapse thresholds due to preceding earthquake damage.

The work presented in this paper makes significant assumptions with regards to both the structural modeling and the tsunami loading but is based on fundamental structural dynamics and current state-of-art in tsunami load characterization. Further work is required to verify the results of this paper for more realistic structures, to account for the effects of structural characteristics on tsunami loading (e.g. openings) and to extend this work to sequences of earthquake and tsunami loads.

5. ACKNOWLEDGEMENTS

The authors would like to thank the European Research Council for supporting the time of Tiziana Rossetto and Crescenzo Petrone on the work undertaken for this paper under the URBAN WAVES project (ERC Starting Grant: 336084). Joshua Macabuag would like to thank the EPSRC Engineering Doctorate Programme in Urban Sustainability and Resilience held at University College London, and the Willis Research Network for supporting his research time on this paper.

6. REFERENCES

- Arikawa, T., Shimosako, K., & Ishikawa, N. (2012). Structural failure by impulsive tsunami force. In 5th International Conference on Protection of Structures against Hazards (pp. 1–14).
- ASCE 7-16. (2016). ASCE 7 standard Minimum Design Loads and Associated Criteria for Buildings and Other Structures.
- Bahmanpour, Alireza; Eames, I. (2016). Tsunami-induced force and surface pressure on multiple rectangular buildings in an unsteady free-surface channel flow. APS Division of Fluid Dynamics.
- Chock, G., Carden, L., Robertson, I., Olsen, M., & Yu, G. (2013). Tohoku Tsunami-Induced Building Failure Analysis with Implications for U.S. Tsunami and Seismic Design Codes. *Earthquake Spectra*, 29(S1), S99–S126. <https://doi.org/10.1193/1.4000113>
- Dias, W., Yapa, H., & Peiris, N. (2009). Tsunami vulnerability functions from field surveys and Monte Carlo simulation. *Civil Engineering and Environmental Systems*, (26), p181-194.
- Foster, A. S. J., Rossetto, T., & Allsop, W. (2017). An experimentally validated approach for evaluating tsunami inundation forces on rectangular buildings. *Coastal Engineering*.
- Guha-Sapir, D., Below, R., & Hoyois, P. (2015). EM-DAT: international disaster database. Retrieved from <http://www.emdat.be/database>
- Macabuag, J., Rossetto, T., & LLoyd, T. (2014). Sensitivity Analysis of a Framed Structure Under Several Tsunami Design-Guidance Loading Regimes. In 2nd European Conference on Earthquake Engineering and Seismology. Istanbul.
- McKenna, F., Scott, M. H., & Fenves, G. L. (2010). Nonlinear Finite Element Analysis Software Architecture Using Object Composition. *Journal of Computing in Civil Engineering*, 24(1), 95–107.
- MLIT. (2011). Further Information Concerning the Design Method of Safe Buildings that are Structurally Resistant to Tsunamis - Technical Advice No. 2570.pdf.
- Nistor, I., Palermo, D., Cornett, A., & Al-Fae, T. (2010). EXPERIMENTAL AND NUMERICAL MODELING OF TSUNAMI LOADING ON. *Coastal Engineering Proceedings*, 32, 1–14. <https://doi.org/http://dx.doi.org/10.9753/icce.v32.currents.2>
- Nouri, Y. (2008). The Impact of Hydraulic Bores and Debris on Free Standing Structures. University of Ottawa.
- Nouri, Y., Nistor, I., Palermo, D., & Cornett, A. (2010). Experimental Investigation of Tsunami Impact on Free Standing Structures. *Coastal Engineering Journal*, 52(1), 43–70. <https://doi.org/10.1142/S0578563410002117>
- Petrone, C., Rossetto, T., & Goda, K. (2017). Fragility assessment of a RC structure under tsunami actions via nonlinear static and dynamic analyses. *Engineering Structures*.
- Qi, Z. X., Eames, I., & Johnson, E. R. (2014). Force acting on a square cylinder fixed in a free-surface channel flow. *Journal of Fluid Mechanics*, 756, 716–727. <https://doi.org/10.1017/jfm.2014.455>
- R Development Core Team. (2008). R: A language and environment for statistical computing. Vienna, Austria. Retrieved from <http://www.r-project.org>.
- Robertson, I. N., & Riggs, H. R. (2011). OMAE2011-49487 Tsunami Bore Forces on Walls. In Proceedings of the ASTM 2011 30th International Conference on Ocean, Offshore and Arctic Engineering.
- Yeh, H., Barbosa, A. R. ., Ko, H., & Cawley, J. G. (2014). TSUNAMI LOADINGS ON STRUCTURES: REVIEW AND ANALYSIS. *Coastal Engineering Proceedings*, 34. <https://doi.org/http://dx.doi.org/10.9753/icce.v34.currents.4>